Differential Boundary-Layer Analysis and Runback Water Flow Model Applied to Flow Around Airfoils with Thermal Anti-ice

Guilherme Araujo Lima da Silva* Otávio de Mattos Silvares,†

Euryale Jorge Godoy de Jesus Zerbini‡

Escola Politécnica, University of São Paulo, São Paulo, SP, 05508-900. Brazil

Hamid Hefazi§ Hsun-Hu Chen¶

Kalle Kaups‖

California State University Long Beach, Long Beach, California, 90840

Certification regulations require safe flight under icing conditions, therefore, ice protection on aircraft wings and horizontal stabilizers will be necessary if critical aerodynamic performance degradation is to be avoided. The present paper developed a numerical code for prediction of heat and mass transfer in two-phase flow around aeronautical airfoils. These systems are equipped with thermal anti-ice systems that are designed to keep the surface free of ice as much as possible. The code is able to estimate the temperatures and runback water around the airfoil surface due implementation of heat transfer submodels in a baseline thermal anti-ice model: 1) it estimated the airfoil surface wetness factor by means of a runback water film and rivulets pattern flow models; 2) it evaluated the laminar and turbulent boundary layers with pressure gradient and laminar-turbulent transition over non-isothermal and permeable airfoil surfaces by performing integral and differential boundary layer analysis; and 3) it predicted the onset position and length of the laminar-turbulent transition region with pressure gradient and turbulence level effects. The work followed a validation and verification process during the numerical code development. All submodels results were separately verified against experimental data. The numerical results of the thermal performance of the airfoil with the anti-ice baseline model, plus the present contributions, were validated against experimental data of an electrically heated NACA 0012 airfoil operating in the Icing Reseach Tunnel (IRT), NASA, USA.

Nomenclature

A = finite volume area exposed to flow around the airfoil, m^2
B_h = heat transfer driving force
B_m = mass transfer driving force
h = convective heat transfer coefficient,$W/(m^2 \cdot K)$
c_p = specific heat, $J/(kg \cdot K)$
E = mechanical energy, J
e = mechanical energy per unit of film width, J/m

*Ph.D., alumnus of Mechanical Engineering, Av. Prof. Mello Moraes, 2231, now at ATS4i Aero-thermal Solutions for Industry, São Paulo, gasilva@ats4i.com.br, AIAA Member

†Ph.D., Professor, Mechanical Engineering, Av. Prof. Mello Moraes, 2231, also Dean at Instituto Mauá de Tecnologia, Praca Mauá, 1., São Caetano do Sul, Brazil

‡Ph.D., Professor, Mechanical Engineering, Av. Prof. Mello Moraes, 2231.

§Ph.D., Professor and Chair, Mechanical and Aerospace Engineering, 1250 Bellflower Boulevard, Senior AIAA Member

¶Ph.D., Professor, Mechanical and Aerospace Engineering, 1250 Bellflower Boulevard, AIAA Member

‖Emeritus Professor, Mechanical and Aerospace Engineering,1250 Bellflower Boulevard

F = wetness factor
F_r = rivulets flow wetness factor
F_s = stream wise wetness factor
G = mass flux $\rho \cdot u_e$, kg/(s $\cdot$ m^2)
$g(\theta_0)$ = auxiliary function, $-1/4\cos^3\theta_0 - 13/8\cos\theta_0 + 15\theta_0/8\sin\theta_0 - 3/2\theta_0\sin\theta_0$
g_m = mass transfer conductance, kg/(s $\cdot$ m^2)
h = convection heat transfer coefficient, $W/(m^2 \cdot K)$
h = water film height at film break-up position, m
h^+ = non-dimensional critical film height at film break-up position, $(\rho\tau^2 h_0^3)/(6\mu^2\sigma_{fg})$
h_0 = critical film height at break-up position, m
h_r = rivulet height downstream break-up position, m
$h(x)$ = half rivulet height in function of its horizontal coordinate,$R(\cos\theta - cos\theta_0)$, m
i = specific enthalpy, J/kg
k = thermal conductivity, W/(m $\cdot$ K)
$\dot{m}$ = mas flow rate, kg/s
Ma = Mach number
p = pressure, Pa
p_{mixt} = total mixture pressure, Pa
p_{vap} = partial vapor pressure, Pa
$\dot{q}''$ = heat flux, W/m^2
$\dot{q}_{lost}$ = heat transfer rate lost to gaseous flow, W
R = rivulets radius, m
r = high speed aerodynamic recovery factor
R_m = mean rivulet radius within the finite volume, $1/2 \cdot (R_{out} + R_{in})$, m
R_t = thermal resistance, K/W
s = stream wise distance over airfoil surface, m
St = Stanton number, $h/(u \cdot \rho \cdot C)$
T = temperature, K
U = overall heat transfer coefficient, W/(m$^2\cdot$ K)
v_f = liquid water film velocity, m/s
$\bar{v}_f$ = liquid water film mean velocity, m/s
x = half rivulet horizontal coordinate, $0 \leq x \leq R\sin\theta_0$, m
x_{H2O} = water vapor mass fraction in air
y = distance normal to airfoil surface, m
β = local collection efficiency
Δs = finite volume length in stream wise direction, m
ΔT = temperature difference between gaseous flow interface and external flow, K
δ_f = liquid water film height, m
λ_p = pressure gradient parameter, $\theta^2/\nu \cdot du_e/ds$
λ = rivulets center-to-center spacing, m
μ = dynamic viscosity, Pa $\cdot$ s
ν = kinematic viscosity, m^2/s
$\phi(\theta_0)$ = auxiliary function, $\sin\theta_0 - \frac{1}{3}\sin^3\theta_0 - \theta_0\cos\theta_0$
φ = angle between the droplet trajectory and airfoil surface normal at impact point
ξ = rivulet liquid-gas interface correction factor, $\theta_0/\sin\theta_0$
ρ = density, kg/m^3
σ = surface tension, N/m
τ = shear stress applied on liquid water film surface by gaseous flow, Pa
θ = half rivulet angular coordinate, $0 \leq \theta \leq \theta_0$
θ_0 = rivulet contact angle

Subscripts

air = gaseous flow
anti-ice = ice protection heating
d = supercooled water droplet
e = external edge of boundary layer

∞ = freestream, non-disturbed flow
G = location at external gaseous flow
imp = water droplets impingiment
in = finite volume inlet
int = liquid-gas, if wet, or solid-gas interface, if dry
K = kinetic
lam = laminar flow
ls = liquid-solid
lv = liquid-vapor saturation
lv = liquid-vapor
out = finite volume outlet
rec = recovery
ref = reference for water properties T=273.15 K
S = surface
S = location just above liquid water film
T = total
t = end of transition region
$turb$ = turbulent flow
$wall$ = airfoil solid surface
$water$ = liquid or vapor water

Symbols

ρ = specific mass, kg/m^3

Superscripts

$*$ = indicates the blowing effect in gaseous flow local Stanton number

I. Introduction

One of the most known causes of air accidents under adverse atmospheric conditions is the ice accretion on aicraft lifting surfaces, probes and engines. In some cases, if a wing is not protected, ice will form and lead to a critical degradation of aerodynamic performance characteristics. The general concepts in ice formation and prevention are decribed by Silva.[1]

There are two strategies for thermal ice protection systems: 1) *de-ice*: Heaters are periodically activated to melt and remove the ice layers formed during the exposition period, therefore, it works by alternating heating and cooling transients; 2) *anti-ice*: Heaters are constantly activated to prevent ice formation; therefore, it operates in a steady-state regime. Some system architectures, like the Goodrich's Low Power Electrical De-icing (LPED), use both strategies in different heating zones depending on the overall heat transfer demanded. Usually the stagnation region, which has the highest local water collection efficiency, is constantly heated and operates in anti-ice mode. Other downstream heater pannels, located in regions with low or no water catch, operate in de-icing mode.[2] In order to reduce the maxium electrical current demand, the de-icing heaters are not turned on and off at same time but in a controlled sequence to minimize instantaneous power consumption and provide adequate protection. This type of low power system was applied to an composite engine inlet by a large aircraft manufacturer.[3]

The thermal anti-ice systems keep the protected surface temperatures above the water freezing point (0°C). In most systems, the heating panels are distributed span wise and each one may have several independently controlled heating elements distributed stream wise. Depeding on electrical power density provided, three operational regimes are identified: 1) *fully evaporative*: the supplied heating power largely overcomes the cooling demand imposed by ambient conditions; the water is vaporized from upstream the droplet impingement limits; there are no runback water downstream impingement limits; 2) *evaporative*: the heating power is higher than the cooling demand; the runback water evaporates from downstream the impingement limts but from upstream the end of the protected area; 3) *running wet*: the heating power is equal or smaller than the cooling demand; the water flows downstream from the protected area and form runback ice.

A numerical tool for airfoil anti-ice thermal simulation may be applied during the conceptual, design, joint development and certification phases. The requirements of accuracy and processing (CPU) time varies

along the product development phase cycle. The later is the phase, the more accurate the numerical tool. For instance, in the conceptual phase, the code must be fast to allow optmization and batch running in less than a day. During certification, a useful tool defines the critical cases matrix and plan the ground and flight test campaigns. If the numerical results are validated, the cost and duration of icing tunnel and natural icing flight tests will be reduced.

II. Previous Works

Table 1 presents the works reviewed in present research and compares them to the model developed by Silva[4] and published herein. The ANTICE code does not have a boundary layer model to calculate local friction and convective heat transfer coefficient distributions. Therefore, despite it does not have transition prediction model, it included an innovative runback film and rivulets flow model developed by one of its authors.[5]

Classic icing codes have integral boundary layer analyses to model the heat transfer caused by flow over isothermal and fully rough icing surfaces. If used in anti-ice simulations, those routines will overestimate h_{air} because water film and rivulets height are orders of magnitude smaller than equivalent sand grain roughness during icing.[6–8] Other inacuracies in h_{air} may be added because classic icing codes assume isothermal surface and abrupt laminar-turbulent transition triggered by sand grain roughness height.[9]

Table 1 shows that several authors applied differential boundary layer analyses to icing[10,11] and ice protection[12,13] problems. Others used finite difference to calculate h_{air} and C_f around three dimensional bodies and wings.[14] However, they did not have a runback film and rivulets model, a transition onset prediction that considered turbulence level, and a compressible and transpired boundary layer calculation.

Table 1. Previous Works Overview

		Characteristics			
Code	**Authors**	**Boundary-Layer**	**Surface Wetness**	**Transition Region**	**Transition Onset and End**
classic icing codes	various[6–8]	fully rough, incompressible, non-transpired, isothermal, integral	-	abrupt	sand grain roughness
Fortified LEWICE	Cebeci, Chen, Alemdaroglu[10,11]	incompressible, fully rough, non-transpired, differential[15]	-	intermittency[16]	fixed
ANTICE	Al-Khalil et al.[17]	-	film and rivulets flow pattern[5]	-	-
ONERA	Henry[13]	incompressible, smooth, non-transpired, differential	-	-	-
CANICE FD	Morency, Tezok Paraschivoiu[12]	incompressible, smooth, non-transpired, differential[15]		intermittency[16]	*Reynolds Number* effects[18]
previous models	Silva, Silvares Zerbini[19–21]	incompressible, smooth, transpired, non-isothermal, integral[22]	-	intermittency[23]	fixed
present model	Silva[4] and present paper	compressible, smooth, transpired, differential[24]	film and rivulets flow pattern[25]	intermittency[26]	*Reynolds Number*, pressure gradient and turbulent level effects[26]

III. Objective

The present work implemented sub-models to: 1) estimate the airfoil surface wetness factor by adopting a liquid water film flow model as well as a rivulet formation and flow model; 2) evaluate laminar and turbulent boundary layers with pressure gradient and laminar-turbulent transition over non-isothermal and permeable airfoil surfaces by implementing differential boundary layer analysis and 3) predict the onset position and length of the laminar-turbulent transition region.

IV. Overview of Airfoil Anti-ice Simulation

This paper uses the baseline anti-ice thermal model developed and validated previously by Silva, Silvares and Zerbini.[20,21] It applies the First Law of Thermodynamics to liquid water flow and airfoil surfaces and also the Conservation of Mass and Momentum to liquid water flow. The airfoil surface wetness factor distribution is calculated by water film breakdown and rivulet formation developed previously[27] but with constant rivulet spacing, λ. In addition, the transition onset prediction and differential analysis of compressible boundary layers were implemented.[4,28]

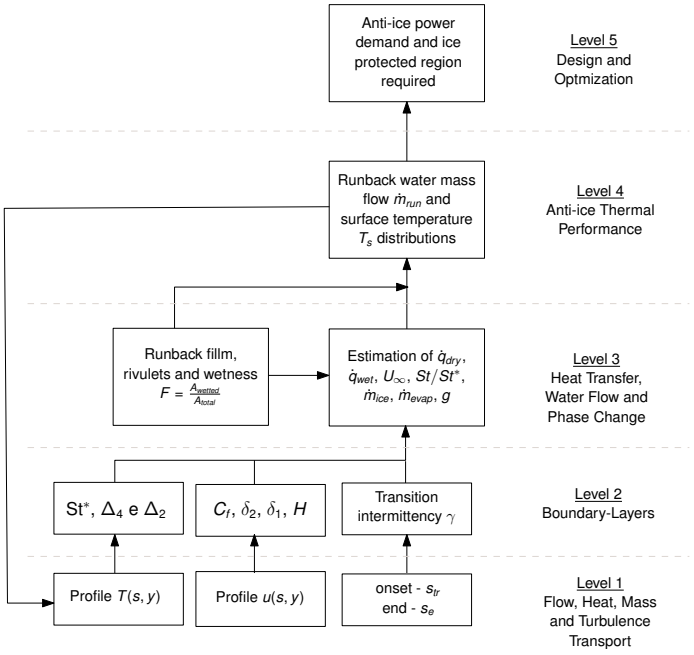

Figure 1. Modeling Levels of Anti-ice Thermal Performance

A. Solvers

The anti-ice simulation problem requires the solution in a sequence of steps : (step 1) velocity and pressure fields around the airfoil; (step 2) droplet impingement on airfoil; (step 3) momentum and thermal boundary layers to obtain the coupled heat and mass transfer over the airfoil solid surface and liquid water flow; (step 4) runback water film breakdown and rivulets formation by minimum total mechanical energy method; (step 5) First Law of Thermodynamics to the liquid water and airfoil solid surface plus the Conservation of Mass and Momentum to the liquid water flow (film and rivulets) over the airfoil.

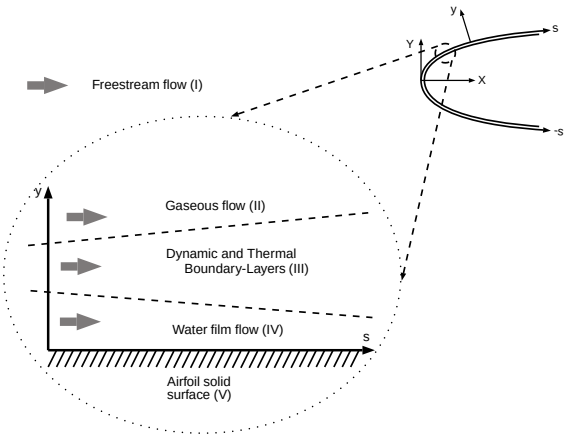

Figure 2. Domains of the Model

Both flow fields around the airfoil and local collection efficiency data were provided by external numerical codes (steps 1 and 2) such as Metacomptech's CFD++ or other solvers. The momentum and thermal boundary layer are evaluated (step 3) in order to estimate the convective heat and mass transfer around the non-isothermal and transpired airfoil surfaces with a smooth laminar-turbulent transition occurrence.The wetness factor distribution downstream the runback water film breakdown position is estimated by a rivulet formation and flow model (step 4). With data from previous steps, the anti-ice mathematical model (step 5) is able to predict operational parameters like solid surface temperatures, runback mass flow rate and convection heat transfer coefficient distributions along the airfoil solid surface. The present paper presents modeling strategies for the thermal boundary layer and runback water flow (step 3 and 4).

B. Modeling Levels

At least five mathematical modeling levels, which are shown in Fig. 1, can be identified in anti-ice system thermal performance modeling: 1) flow, heat, mass and turbulence transport: where the reynolds-averaged navier-stokes equations are solved coupled with energy equation for compressible boundary layer flow conditions; 2) boundary layers: where the momentum and thermal compressible boundary layers around non-isothermal airfoil surfaces are estimated by the finite difference method; 3) heat and mass transfer: where estimates are made for heat transfer rates which consider effects of evaporation, freezing and partially wetted surfaces when they occur; and estimate are made for the film breakdown and rivulets formation. 4) anti-ice thermal performance: where the First Law of Thermodynamics, Convervation of Mass and Momentum are applied to airfoil surface and water runback flow; 5) design and optimization: where the ice protected area and the thermal power demand to prevent ice accumulation on airfoils are defined;

V. Airfoil Anti-ice Thermal Performance Modeling

Figure 2 shows the coordinates system and the five domains used in the present mathematical model: I) free stream flow; II) gaseous flow; III) momentum or thermal boundary layers; IV) water film flow and; V) solid surface. By using this strategy for domain division, the mathematical model can be organized and simplified.

The First Law of Thermodynamics applied to solid surface (domain V) results:

$$\frac{d}{ds}\left(k_{wall}\cdot\frac{dT_{wall}}{ds}\right)-F\cdot h_{water}\cdot(T_{wall}-T_{water})+\dot{q}''_{anti-ice}+(1-F)\cdot[-h_{air}\cdot(T_{wall}-T_{rec})]=0 \quad (1)$$

Equation (1) considers conduction heat transfer in the s direction but neglects in the y direction. The heat flux distribution term $\dot{q}''_{anti-ice}$ in Eq. (1) is determined by electrical heater elements.

$$T_{rec}=(1-r)\cdot T_e+r\cdot T_{stag} \quad (2)$$

$$T_e=T_{stag}/\left(1+0.2\cdot \mathrm{Ma}_e^2\right) \quad (3)$$

The recovery factor r is assumed to be $\mathrm{Pr}^{1/2}$ in the laminar regime and $\mathrm{Pr}^{1/3}$ in the turbulent regime. A type of wetness factor F is defined in order to represent the wetted area fraction in the finite volume ($F=1$ if surface of liquid-gas interface is fully wet, $0<F<1$ if it is partially wet, $F=0$ if it is fully dry). The last finite volume at the trailing edge on upper or lower airfoil surface is considered to be adiabatic. The thermodynamic properties of air for high-speed flows can be evaluated at temperature[29]:

$$\bar{T}_{air}=T_e+0.5\cdot(T_{int}-T_e)+0.22\cdot(T_{rec}-T_e) \quad (4)$$

where solid-gas or liquid-gas interface temperature T_{int} can assume the value of T_{wall} or T_{water}, if the airfoil surface is dry or wet, respectively. By applying the First Law of Thermodynamics to the water film flow (domain IV), it is possible to obtain:

$$\begin{aligned}F\cdot A\cdot h^*_{air}\cdot(T_{rec}-T_{water})+F\cdot A\cdot h_{water}\cdot(T_{wall}-T_{water})+\dot{m}_{in}\cdot c_{p,water}\cdot(T_{in}-T_{ref})\\ -\dot{m}_{out}\cdot c_{p,water}\cdot(T_{out}-T_{ref})+\cdot A\cdot\dot{m}_{imp}\cdot\left[c_{p,water}\cdot(T_d-T_{ref})+\frac{V_d^2}{2}\right]\\ +\dot{m}_{evap}\cdot[i_{lv}-c_{p,water}\cdot(T_{out}-T_{ref})]=0\end{aligned} \quad (5)$$

with

$$T_{water}=(T_{in}-T_{out})/2 \quad (6)$$

The convection heat transfer coefficient h_{water}, between water film (IV) and solid surface (V), is calculated by *Colburn* analogy between momentum and heat transfer:

$$h_{water}=\rho_{water}\cdot v_f(s,\delta_f)\cdot c_{p,water}\cdot 0.5\cdot C_f\cdot \mathrm{Pr}_{water}^{-2/3} \quad (7)$$

The water thermodynamics properties are evaluated for low speed flows according to Eckert[29] at temperature:

$$\bar{T}_{water} = T_{wall} + 0.5 \cdot (T_{water} - T_{wall}) \tag{8}$$

By applying the Mass Conservation principle to the water film flow (mathematical domain IV), the following equation is obtained:

$$\dot{m}_{in} + \dot{m}_{imp} = \dot{m}_{out} + \dot{m}_{evap} \tag{9}$$

According to Spalding,[30] the water evaporation mass flux is calculated by:

$$\dot{m}''_{evap} = g_m \cdot \mathrm{B}_m \tag{10}$$

$$g_m = \mathrm{St} \cdot G \cdot \mathrm{Le}^{2/3} \cdot \frac{\ln(1 + \mathrm{B}_m)}{\mathrm{B}_m} \tag{11}$$

where B_m is calculated by the following expressions:[31]

$$\mathrm{B}_m = \frac{x_{H2O,S} - x_{H2O,G}}{x_{H2O,S} - 1} \tag{12}$$

$$x_{H2O,G} = \frac{p_{vap,G}}{1.61 \cdot p_{mixt,G} - 0.61 \cdot p_{vap,G}} \tag{13}$$

$$x_{H2O,S} = \frac{p_{vap,S}}{1.61 \cdot p_{mixt,S} - 0.61 \cdot p_{vap,S}} \tag{14}$$

Where S just above the liquid water film surface and G at gaseous flow around the airfoil.
The heat transfer driving force is defined as:[30–32]

$$\mathrm{B}_h = \frac{\dot{m}''_{evap}}{\mathrm{St}^* \cdot G} \tag{15}$$

For the mass transfer, surface roughness and pressure gradient levels of the reference cases defined herein, the effect of blowing on convective heat transfer is accounted for through:

$$\frac{\mathrm{St}^*}{\mathrm{St}} = \frac{\ln(1 + \mathrm{B}_h)}{\mathrm{B}_h} \tag{16}$$

This is a coupled heat and mass transfer process where St^* depends on B_h, Eq. (16), which depends on both $\dot{m}''_{evap}$ and St^*, Eq. (15). The iterative calculation process only finishes when First Law of Thermodynamics, Eq. (5), is satisfied in each finite volume.
From the water droplet local collection efficiency definition, the impinging water flow is given by:

$$\dot{m}_{imp} = V_\infty \cdot \beta \cdot LWC \cdot \Delta s \cdot 1 \tag{17}$$

At the stagnation point, it is assumed that no runback water enters in the finite volume and the Eq. (9) is solved from the stagnation point to the downstream direction for both the lower and upper airfoil surfaces.
At the finite volume where the T_{water} reaches solidification temperature, it was assumed that no outlet runback water mass flow rate $\dot{m}_{out} = 0$, which denotes the beginning of the water freezing. Neither the effects of solidification enthalpy is considered in Eq. (5) nor is the existence of partially frozen water runback included in Eq. (9). These are crude assumptions to forecast the water freezing location and ice growth; however, they are conservative enough to indicate that the system is not performing adequately. In addition, one of the objectives of the present work is to predict performance of an anti-ice system, which is designed to prevent ice formation and operate at average temperatures higher than $0°C$. If the warming effect due to enthalpy releasing had been considered, the model would have indicated the water freezing initiation in a further position than that which predicted by present model. Al-Khalil[5] used similar conservative assumptions for the freezing process in his basic model.
In order to compare the numerical results of present work with experimental data,[17] an overall heat transfer coefficient U was defined taking into account the effects of the convective heat transfer rate across

solid-liquid and liquid-gas surfaces interfaces (i.e. h_{water} and h_{air}), runback water enthalpy net flux, water droplets impingement enthalpy and evaporation enthalpy:

$$U = \frac{\dot{q}_{lost}}{1 \cdot \Delta s \cdot \Delta T} \tag{18}$$

$$\dot{q}_{lost} = R_t^{-1} \cdot 1 \cdot \Delta s \cdot \Delta T - \dot{m}_{evap} \cdot (i_{lv} + i_{water}) + \dot{m}_{imp} \cdot i_d + \dot{m}_{in} \cdot i_{in} - \dot{m}_{out} \cdot i_{out} \tag{19}$$

The Momentum Conservation equation for the water film in the present case:

$$\frac{1}{\rho_{water}} \cdot \frac{\partial p_e}{\partial s} = \nu_{water} \cdot \frac{\partial^2 v_f(s,y)}{\partial y^2} \tag{20}$$

Equation (20) is solved by applying the boundary conditions at the water film flow (IV):

$$\begin{aligned} y = \delta_f &\Rightarrow \mu_{water} \cdot \left[\frac{\partial v_f(s,y)}{\partial y}\right]_{\delta_f} = \tau + \dot{m}''_{imp} \cdot V_d \cdot \sin\varphi \\ y = 0 &\Rightarrow v(s,y) = 0 \end{aligned} \tag{21}$$

The velocity profile of the water film, after the solution of Eq. (20):

$$v_f(s,y) = \frac{\partial p_e}{\partial s} \cdot \frac{y^2}{2 \cdot \mu_{water}} + \left[\tau + \dot{m}''_{imp} \cdot V_d \cdot \sin\varphi - \delta_f(s) \cdot \frac{\partial p_e}{\partial s}\right] \cdot \frac{y}{\mu_{water}} \tag{22}$$

The water film thickness can be calculated from the mean water film velocity, which is obtained with Eq. (22):

$$\delta_f = \frac{\dot{m}_{in} + \dot{m}_{out}}{2 \cdot \rho_{water} \cdot \bar{v}_f} \tag{23}$$

VI. Surface Wetness Modeling

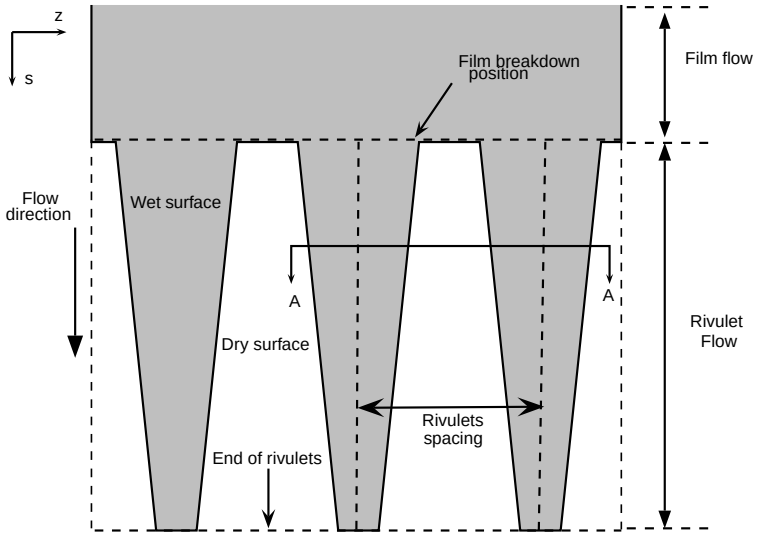

Figure 3. Water Film Breakdown Model

With a thermal anti-ice activated, the water droplets impinge and form a thin water film at the leading edge. Then the runback water flows to downstream regions driven by pressure and shear forces applied by external flow around the airfoil. The film thickness may vary stream wise due to effects of evaporation, external flow pressure gradient, shear stress or heating. If a critical thickness is reached, the water film breaks-up and forms rivulets.

The change from film to a rivulet flow pattern is marked by a decrease in wetted area because dry patches start to grow between rivulets and the airfoil surface becomes directly exposed to gaseous flow around the airfoil. In sum, the rivulet flow affects the effectiveness of the anti-ice system since it decreases the area of heat transfer between the water and the airfoil surface, and also decreases the area of heat and mass transfer between water and the external flow.

From the stagnation point to the impingement region limits, the runback water is assumed to flow as a continuous film. Downstream from those limits, a wetness factor is calculated by using a rivulets formation model[27,28] that adopts the Minimum Total Energy criteria.[25,33] It proposes four equations to find the

critical film thickness, the rivulet wetness factor F_r, rivulet radius and center-to-center rivulet spacing: 1) conservation of mass in the transition between film and rivulet flow patterns in the stream wise direction; 2) conservation of total energy from film to rivulet in the stream wise direction; 3) rivulet total energy minimization; and 4) geometrical relationships. In the present model, the overall wetness factor F is composed by two contributions:

$$F = F_r \cdot F_s \quad \text{where} \quad 0 \leqslant F \leqslant 1 \quad \text{and} \quad F = \frac{A_{wet}}{A_{total}} \quad \text{where} \quad A_{total} = A_{dry} + A_{wet} \tag{24}$$

where the wetness factor F_r is defined as the ratio between the rivulet base width and the distance between two rivulet centers λ, F_s is the ratio of stream wise wetted distance by the finite volume total distance; A_{total} is the total finite volume area exposed to gaseous flow around the airfoil. Thus, F is used to multiply A_{total} associated with water and air convective heat and mass transfer terms in the First Law of Thermodynamics applied to both solid surface and runback water flow.

A. Water Film Breakdown and Rivulets Formation

The MTE criteria[25,33] proposes four equations in order to find the critical film thickness h_0, the rivulet wetness factor F_r, rivulet radius R and center-to-center rivulet spacing λ. The set of equations to be solved is: 1) conservation of mass in the transition between film and rivulet flow patterns in stream wise direction; 2) conservation of total energy ($e_T = e_K + e_S$) from film to rivulet in stream wise direction; 3) rivulet total energy minimization; and 4) geometrical relationships.

An overall wetness factor F is included in the heat and mass transfer parcels of anti-ice system thermal balance equations.[19,34] It is composed of different contributions:

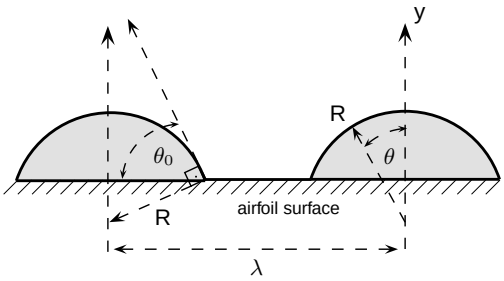

Figure 4. Cylindrical rivulet cross section

$$F = F_r \cdot F_s \tag{25}$$

where F_r is the ratio between the rivulet base width and the distance between two rivulets centers λ, F_s is the ratio of stream wise wetted distance by the finite volume total distance.

From rivulet geometry presented in Fig. 4, the wetness factor caused by rivulet flow F_r is given by:

$$F_r = \frac{2R \sin\theta_0}{\lambda} \tag{26}$$

With the assumption of *Couette* flow velocity profile $v = v(y)$, the mass flow rate of $\dot{m}'_f$ and rivulet $\dot{m}'_r$ are estimated by:[25]

$$\frac{\dot{m}_f}{\lambda} = \dot{m}'_f = \int_0^{h_0} \rho\, v(y) dy = \frac{\rho\tau}{2\mu} h_0^2 \tag{27}$$

$$\frac{\dot{m}_r}{\lambda} = \dot{m}'_r = \frac{2}{\lambda} \int_0^{R\sin\theta_0} \int_0^{h(x)} \rho\, v(x,y) dx dy = \frac{\rho\tau}{\mu} \frac{\phi(\theta_0)}{\lambda} R^3 \tag{28}$$

Then, the total mechanical energy of film e_f and rivulets e_r may be approximately described:[25]

$$\frac{E_f}{\lambda} = e_f = \int_0^{h_0} \frac{\rho}{2} u^2(y) dy + \sigma_{lv} + \sigma_{ls} = \frac{\rho\tau^2}{6\mu^2} h_0^3 + \sigma_{lv} + \sigma_{ls} \tag{29}$$

$$\frac{E_r}{\lambda} = e_r = \frac{\rho}{\lambda} \int_0^{R\sin\theta_0} \int_0^{h(x)} u^2(x,y)dxdy + \left(\frac{2R\theta_0}{\lambda} + \cos\theta_0 - \frac{R\sin 2\theta_0}{\lambda}\right)\sigma_{lv} + \sigma_{ls} =$$

$$\frac{\rho\tau^2}{6\mu^2} g(\theta_0) h_0^3 \left(\frac{\sin\theta_0}{\phi(\theta_0)}\right)^{3/2} F_r^{-1/2} + \left(F_r \frac{\theta_0}{\sin\theta_0} + \cos\theta_0 - F_r\cos\theta_0\right)\sigma_{lv} + \sigma_{ls} \quad (30)$$

The application of the mass and total mechanical energy conservation principles to the transition from film to rivulet flow pattern,i.e., Eq. (27) equals to Eq. (28) and Eq. (29) equals to Eq. (30), results:

$$R = h_0 \left(\frac{\sin\theta_0}{\phi(\theta_0)F_r}\right)^{1/2} \quad (31a)$$

$$h^+ g(\theta_0) \left(\frac{\sin\theta_0}{\phi(\theta_0)}\right)^{3/2} F_r^{-1/2} + \left(\frac{\theta_0}{\sin\theta_0} - \cos\theta_0\right) F_r - (1-\cos\theta_0) - h^+ = 0 \quad (31b)$$

The more stable rivulet flow pattern is found by the total mechanical energy minimization in relation to the wetted area fraction F_r:

$$\frac{\partial e_r}{\partial F_r} = 0 \; and \; \frac{\partial^2 e_r}{\partial F_r^2} > 0 \quad (32)$$

With the equation system composed by Eq. (31) and the minimization of Eq. (30) according to MTE criteria of Eq. (32), the non-dimensional film critical height h^+ equation is found:

$$h^+ = (3.2)^{-3/2} \cdot \left(\frac{\theta_0}{\sin\theta_0} - \cos\theta_0\right) \cdot \left[h^+ \cdot g(\theta_0)\right]^{2/3} \cdot \frac{\sin\theta_0}{\phi(\theta_0)} - (1-\cos\theta_0) \quad (33)$$

At the impingement limits, the rivulet geometry relations and the *MTE* criteria equations given by Eq. (26), Eq. (31) and Eq. (32) provide F_r, R, λ and h_0. However, if the critical film thickness is reached ($\delta_f \leq h_0$) inside the impingement region, the film is assumed to not break due to effects of multiple droplet impacts and spreading.

When the continuous film height is smaller than the critical height upstream from the impingement limit position, $\delta_f < h_0$, the minimization of the total mechanical energy criteria of Eq. (32) is no longer applied since the critical film height is considered to be the film height $h_0 = \delta_f$. Therefore the only equations used are the geometry relations Eq. (26) and the total mechanical energy and mass conservation Eq. (31). This equation system is sufficient to find F_r, R and λ since h_0 is already known.

B. Rivulets Flow

At downstream regions of the film break-up position, the rivulet flow pattern parameters (R, F_r and λ) are calculated with Eq. (26), Eq. (28) and the mass conservation principle applied to rivulet flow. By assumption, there is no impingement at region of rivulet flow :

$$\dot{m}'_{r,in} = \dot{m}'_{r,out} + \dot{m}'_{r,evap} \quad (34)$$

By assuming μ, ρ, τ, θ_0 and F_r constants within each finite volume and using Eq. (26) Eq. (28), Eq. (34) and Eq. (37), the following equation system is obtained:

$$R_{out}^2 = R_{in}^2 + \frac{2\mu\theta_0}{\rho\tau\phi(\theta_0)} \cdot (-\dot{m}''_{r,evap} \cdot \Delta s) \quad (35a)$$

$$F_r = 1/2 \cdot (\dot{m}'_{r,in} + \dot{m}'_{r,out}) \cdot \frac{2\mu\sin\theta_0}{\rho\tau\phi R_m^2} \quad (35b)$$

$$\lambda \Rightarrow \text{constant} \quad (35c)$$

where

$$\frac{\dot{m}_{r,evap}}{\lambda} = \dot{m}'_{r,evap} = \dot{m}''_{r,evap} \cdot \Delta s \cdot F_r \cdot F_s \cdot \xi \tag{36}$$

The factor ξ is the ratio between the exposed area of the segment of cylinder rivulet and its base width (correction to compensate the rivulet top surface curvature). According to Fig. 4, this factor is equal to:

$$\xi = \frac{2R\theta_0}{2R\sin\theta_0} = \frac{\theta_0}{\sin\theta_0} \tag{37}$$

The rivulet radius R correlates with rivulet height h_r (distance from base to top of segment of cylinder) and:

$$h_r = R \cdot (1 - \cos\theta_0) \tag{38}$$

Thus, the runback water flow height distribution around the airfoil is given by values of: a) δ_f at regions upstream from the impingement limits; b) h_0 at film break-up position; c) h_r at regions downstream from the impingement limits.

VII. Dynamic and Thermal Boundary-Layers Modeling

The present paper applies the finite difference method to solve the Reynolds-averaged *Navier-Stokes* (RANS) simplified for boundary layer flows. This method takes into account the flow history effects that are not considered by integral analysis like stream wise surface temperature gradients caused by anti-ice heating and pressure gradient variations due to flow acceleration from stagnation to downtream airfoil regions.

The code BLP2C[24] solves the coupled momentum and energy conservation equations for two dimensional compressible boundary layer flows in laminar, transitional and turbulent regimes:

- mass conservation:

$$\frac{\partial}{\partial x}(\rho u) + \frac{\partial}{\partial y}(\overline{\rho v}) = 0 \tag{39}$$

- momentum conservation (RANS for boundary layer) :

$$\rho u\frac{\partial u}{\partial x} + \overline{\rho v}\frac{\partial u}{\partial y} = -\frac{dp}{dx} + \frac{\partial}{\partial y}\left(\mu\frac{\partial u}{\partial y} - \rho\overline{u'v'}\right) \tag{40}$$

- energy conservation (First Law of Thermodynamics):

$$\rho u\frac{\partial H}{\partial x} + \overline{\rho v}\frac{\partial H}{\partial y} = \frac{\partial}{\partial y}\left[k\frac{\partial T}{\partial y} - c_p\rho\overline{T'v'} + u\left(\mu\frac{\partial u}{\partial y} - \rho\overline{u'v'}\right)\right] \tag{41}$$

- pressure in the boundary layer edge by incompressible, isentropic flow:

$$-\frac{dp}{dx} = \rho_e u_e\left(\frac{du_e}{dx}\right) \tag{42}$$

- eddy viscosity definition:

$$-\overline{u'v'} = \epsilon_m\frac{\partial u}{\partial y} \qquad \text{and} \qquad -\overline{T'v'} = \frac{\epsilon_m}{\mathrm{Pr}_t}\frac{\partial u}{\partial y} \tag{43}$$

- algebraic turbulence model:[35]

$$(\epsilon_m)_i = l^2 \left|\frac{\partial u}{\partial y}\right|^2 \gamma_{tr}\gamma, \qquad 0 \le y \le y_c \tag{44}$$

$$(\epsilon_m)_o = 0.0168 \left|\int_0^\infty (u_e - u)dy\right| \gamma_{tr}\gamma, \qquad y_c \le y \le \delta \tag{45}$$

$$(\epsilon_m)_o = (\epsilon_m)_i, \qquad y = yc \tag{46}$$

$$l = \kappa y \left[1 - \exp\left(-\frac{y}{A}\right)\right], \qquad N = \left[1 - 11.8\frac{\mu_w}{\mu_e}\left(\frac{\rho_e}{\rho_w}\right)^2 p^+\right]^{1/2} \tag{47}$$

$$A = 26\frac{\nu}{N}u_T^{-1}\left(\frac{\rho}{\rho_w}\right)^{1/2}, \quad u_T = \left(\frac{\tau_w}{\rho_w}\right), \quad p^+ = \frac{\nu_e u_e}{u_T^3}\frac{du_e}{dx}, \quad v_w^+ = \frac{v_w}{u_T} \tag{48}$$

- intermitency from the inner to the outer boundary layer flow:

$$\gamma = \left[1 + 5.5\left(\frac{y}{y_0}\right)^6\right]^{-1}, \qquad y_0 \text{ is defined at } \frac{u}{u_e} = 0.995 \tag{49}$$

VIII. Laminar-Turbulent Transition Modeling

In terms of the mean effect of heat and mass transfer over the airfoil surface, both laminar-turbulent transition onset position, s_{tr}, and transition region extension are important parameters when predicting the thermal performance of anti-ice systems. The laminar part have to be considered because the area covered by laminar flow may be significant when compared with the total ice protected area. Moreover, the transition may occur within the airfoil heated area over the runback flow, therefore, it will affect locally the heat and mass transfer fluxes.

The anti-ice system thermal performance is defined by the position where the water evaporates or freezes, i.e., it is given by the local values of T_s and runback water flow $\dot{m}_{water}$ around the airfoil. Both depend on the history of the local coefficient of heat transfer along airfoil's upper and lower protected surfaces.

Sogin[36] made pioneer flight and tunnel observations about the importance of laminar-turbulent transition effects on the airfoils thermally protected against ice formation. Recently other researchers confirmed conclusions about heat transfer and transition modeling relevance for simulation and design of anti-ice systems.[1,9,17,37,38] Experimental evidences[39] and numerical results[40] also confirmed the major role of transition during icing formation on unheated airfoils at certain conditions.

The present paper adopts a set of algebraic correlations to estimate the onset and extension of the transition region that considers effects of *Reynolds number*, pressure gradient and freestream turbulence level, which can vary according experimental conditions in tunnel or in flight:

$$Re_{\delta_{2.tr}} = 163 + \exp\left(F(\lambda_p) - \frac{F(\lambda_p)}{6.91} \cdot Tu\right) \tag{50}$$

where λ_p is a sort of pressure grandient parameter, $F(\lambda_p)$ is estimated by Eq. (51a) for $\lambda_p < 0$ and by Eq. (51b) for $\lambda_p > 0$:

$$F(\lambda_p) = 6.91 + 12.75 \cdot \lambda_p + 63.64 \cdot \lambda_p^2 \tag{51a}$$

$$F(\lambda_p) = 6.91 + 2.48 \cdot \lambda_p - 12.27 \cdot \lambda_p^2 \tag{51b}$$

The end of the transition region and beginning of fully turbulent flow is estimated by correlations:

$$Re_{\delta_2,t} = 540 + 183.5 \cdot \left(Re_L \cdot 10^{-5} - 1.5\right)\left(1 - 1.4 \cdot \lambda_p\right) \tag{52a}$$

$$Re_L = 16.8 \cdot \left(Re_{s,tr}\right)^{0.8} \tag{52b}$$

Based on a comprehensive experimental data set, the authors proposed an intermitency function:[26]

$$\gamma_{tr} = 1 - \exp\left(-5\eta^3\right) \qquad \text{and} \qquad \eta = \frac{\mathrm{Re}_s - \mathrm{Re}_{s,tr}}{\mathrm{Re}_{s,e} - \mathrm{Re}_{s,tr}} \tag{53}$$

The difference $(s_e - s_{tr})$ is the extension of the transition region. This model is an algebraic transition model and multiplies the intermittency by the eddy viscosity, Eqs. (44) e (45). In the present work, the Abu-Ghannam and Shaw correlations,[26] which were originally intented to be applied in transition linear combination models, is used herein in an algebraic model. One advantage of those correlations is the ability to predict transition parameters in a wide range of conditions, from natural to bypass transition process paths.

Table 2. Experimental Cases[17]

Parameter	22A	67A and 67B
V_∞ [m/s]	44.7	89.4
T_{tot} [°C]	-7.6	-21.6
α	0°	0°
LWC [g/m^{-3}]	0.78	0.55
MVD [μm]	20	20
$(s/c)_{prot}$	$\approx 10\%$	$\approx 10\%$
$\mathrm{Re}_{c.prot}$	$6.72 \cdot 10^5$	$1.38 \cdot 10^6$
M	0.1369	0.2813

The onset position s_{tr} predicted by Eq. (50) is not the concentrated breakdown or the abrupt transition. The model assumes that most turbulent spot generations are distributed in a tiny range just downstream from s_{tr}.

One of the present authors implemented the Abu-Ghannam & Shaw transition and intermittency models[26] into BLP2C code in his Ph.D. thesis development.[4] Its results were compared with experimental data and other numerical results of integral analysis with linear combination models and finite volume differential analysis (CFD commercial code) with intermittency transport equations.[41]

IX. Test Cases

Al-Khalil *et al.*[17] performed anti-icing experiments at the Icing Research Tunnel at NASA Glenn Research Center facilities, Cleveland, Ohio, USA, by measuring the surface temperatures and overall heat transfer coefficients in order to validate ANTICE code numerical results. The airfoil tested was 1.828 m span by 0.914 m chord NACA 0012 profile with electronically controlled heaters. Each heater element in the stream wise direction had one thermocouple, one thermoresistor sensor and one heat flux gauge installed. Table 2 presents test cases 22A, 67A and 67B. Table 3 presents the heater element positions and their power densities in each test case.

The heater assembly was composed, from inner to outer surface, by layers of 0.020 mm stainless steel, 0.28 mm elastomer, 0.01 heating resistance, 0.28 mm elastomer, 0.89 mm epoxi and glass fiber and 3.43 mm silicone. The present paper considered the fact that all layers were approximately at the same temperature and their thermal conductivity is represented by $k = 16.27$ W/(m^2·K).

X. Numerical Simulation

The numerical results of the differential analysis, which is described in the present work, and the integral analysis developed in previous work[28] are compared with experimental results.[17] In both differential and integral analyses, we used the same models for rivulet formation and laminar-turbulent transition prediction. The numerical implementation of the anti-ice thermal performance numerical simulator is described in previous works[1,42]

Table 3. Heater positions and power densities[17]

Heater	s/c		$\dot{q}''_{anti}$ [kW/m^2]		
element	start	end	22A	67A	67B
F	−0.1024	−0.0607	9.92	20.15	8.37
D	−0.0607	−0.0329	10.23	21.70	11.93
B	−0.0329	−0.0051	32.55	32.55	10.85
A	−0.0051	0.0157	46.5	43.40	15.19
C	0.0157	0.0435	18.6	26.35	9.92
E	0.0435	0.0713	6.97	18.60	12.86
G	0.0713	0.1129	10.23	18.60	8.68

A. Transition Parameters

The present authors adjusted Tu values in order to get appropriate values of the transition onset and end positions by Eq. (50) and (52a) for each case as shown in Table 4. The adjustment criteria was the smaller deviation between the numerical and experimental values of U and T_s . By correlating Henze, Bragg and Kim[43] results, the tunnel for 22A, 67A and 67B conditions has estimated nominal

freestream value of $Tu = 0.7\%$. Same work mention that IRT turbulence level can increase up to 6% when measured close to the body at the test section.

Some effects may influence the laminar-turbulent transition occurrence when testing airfoil anti-icing systems: 1) roughness generated by runback water film and rivulet flows; 2) surface waviness caused by non-embeded electrical heaters, which may be the case of tests simulated herein; 3) surface temperature levels and their variations in stream wise direction; 4) presence of water droplets in flow around the airfoil and their impact on the surface; and 5) water evaporation.

Table 4. Turbulence Levels Assumed

Case	Integral	Differential
22A	3.1%	4.5%
67A	1.9%	2.7%
67B	3.0%	4.1%

Moreover the turbulence length scales generated in icing tunnel processes may be different from the ones generated at wind tunnels by turbulence grids used to build transition prediction correlations. Another effects may be the position where Tu is defined at NASA IRT and those positions defined in experiments used by Abu-Ghannam & Shaw to fit the data.

Therefore, the Tu may be understood as "equivalent" in present paper because it will represent other surfaces or environment disturbances in addition to the ones considered in semi-empirical correlations.[26]

B. Numerical Results

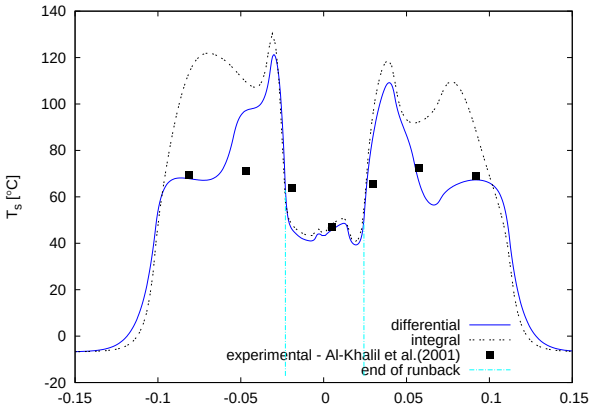

(a) Surface Temperature - T_s

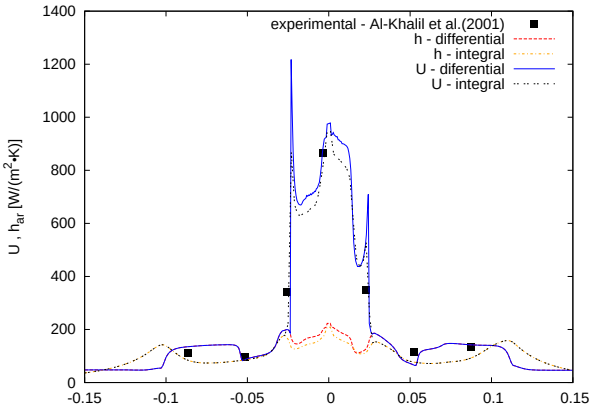

(b) Heat Transfer Coefficients - U e h_{air}

Figure 5. Surface Temperature and Heat Transfer - Case 22A

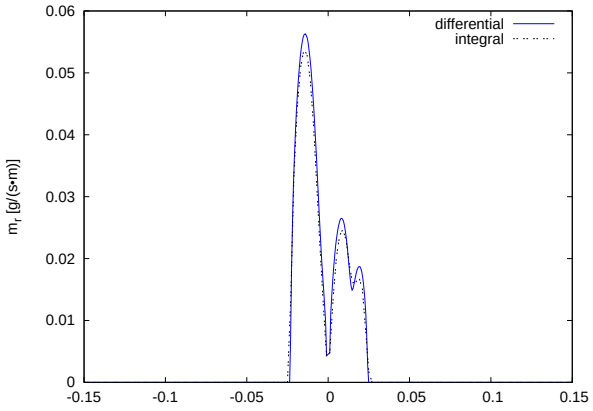

(a) Water Mass Flow Rate - $\dot{m}'_r$

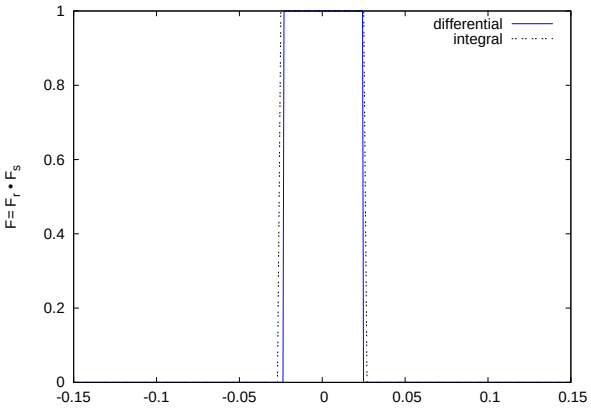

(b) Surface Wetness - F

Figure 6. Runback Water Flow - Case 22A

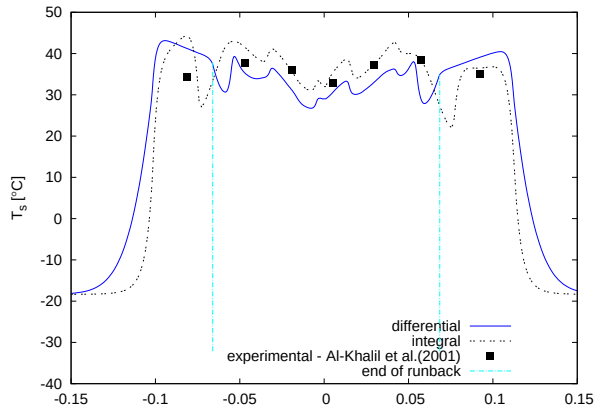

(a) Surface Temperature - T_s

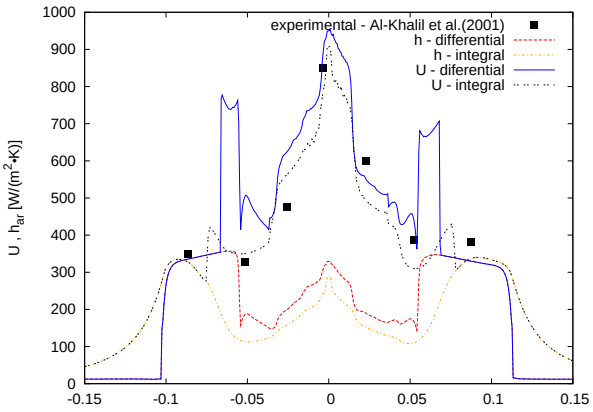

(b) Heat Transfer Coefficients - U e h_{air}

Figure 7. Surface Temperature and Heat Transfer - Case 67A

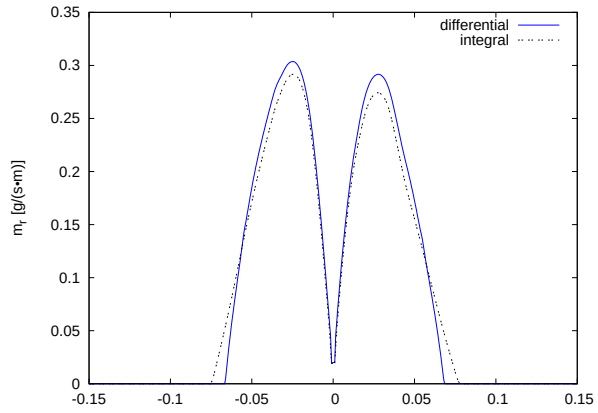

(a) Water Mass Flow Rate - $\dot{m}'_r$

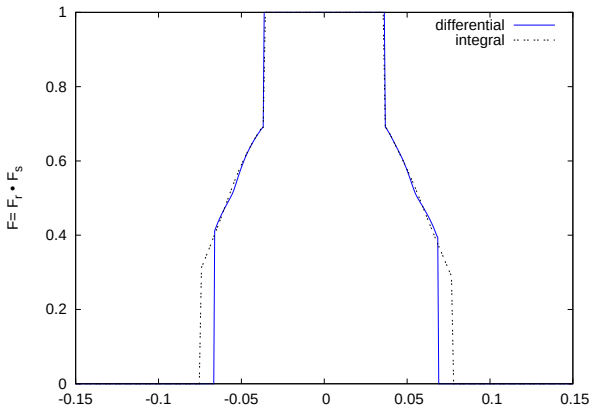

(b) Surface Wetness - F

Figure 8. Runback Water Flow - Case 67A

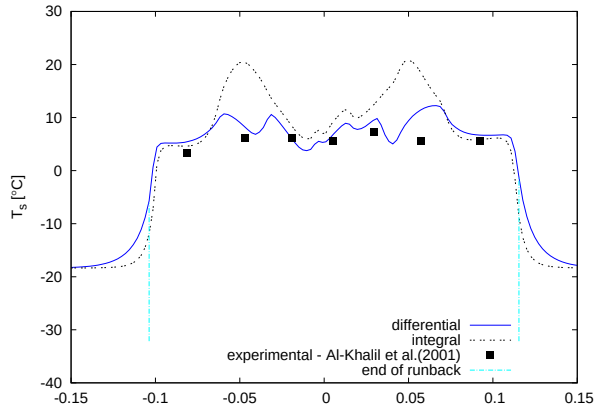

(a) Surface Temperature - T_s

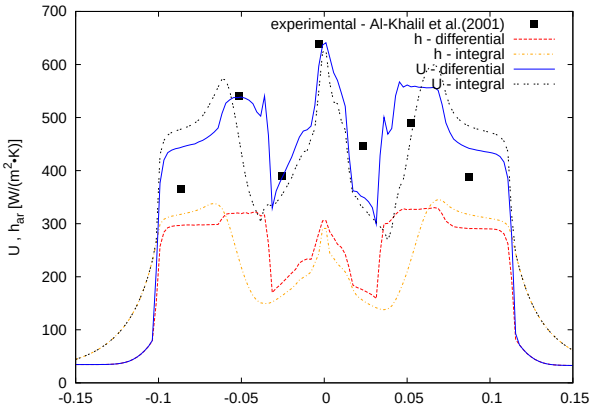

(b) Heat Transfer Coefficients - U e h_{air}

Figure 9. Surface Temperature and Heat Transfer - Case 67B

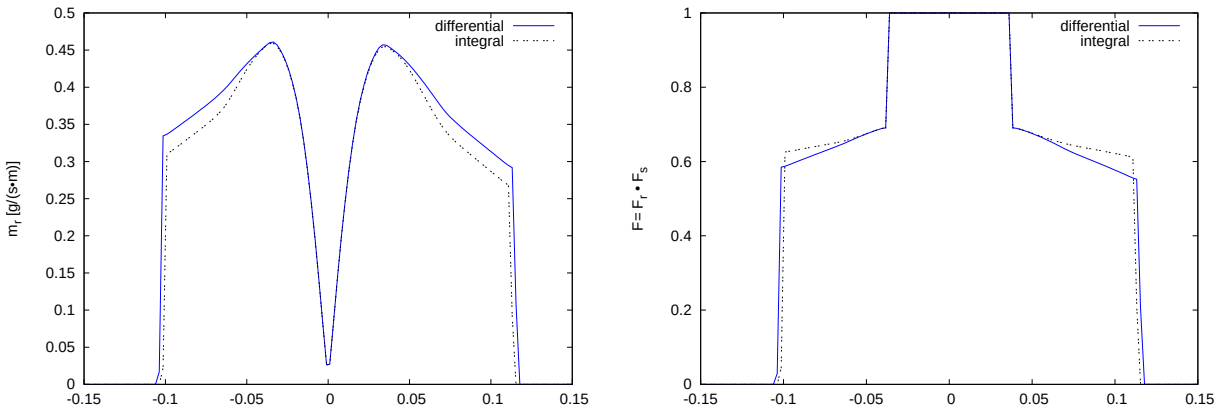

(a) Water Mass Flow Rate - $\dot{m}'_r$

(b) Surface Wetness - F

Figure 10. Runback Water Flow- Case 67B

Figure 5(a) presents surface temperature distribution predicted by the differential presented herein and integral models developed in the previous paper.[28] The numerical results are compared with measurements taken by Al-Khalil *et al.*[17] at NASA IRT. The differential model predicted T_s and U would be closer to experimental data than the integral model as shown in Figs. 5(a) e 5(b). Probably, the Tu difference between differential (3.1%) and integral (4.5%) analyses are due to U estimation in laminar regime region. The differential numerical result is closer to laminar heat transfer exact solution than the integral result, which tends to filter and not capture the effects of rapid surface temperature and pressure gradient variations. Both models estimated similar $\dot{m}_{water}$ and F distributions, Fig. 6, because surface temperatures are at the same levels in the wet region. The main discrepancies are located only at dry areas, downstream from the runback evaporation but upstream from the end of the heating area.

The results of T_s and U for 67A case are presented in Fig. 7. The results are closer to experimental data in the wet regions than the dry ones. Regarding turbulence levels, the differential model required a smaller value of $Tu = 1.9\%$ than that of the integral, $Tu = 2.7\%$. There is a remarkable difference between the local values and the history of U and h_{air} between both models. Figure 8 shows that differential analysis predicted a final evaporation position more downstream than those results of the integral analysis, which means they are more conservative in a design point of view. As the wet region is longer in case 67A than in case 22A, the estimation of U and T_s was more significant in case 67A than 22A.

In case 67B, Tu was 3% in differential and 4.1% in integral analysis. Figure 9 shows that the differential numerical results are closer to experimental data points than integral results. It was not possible to find a Tu value to decrease devitation between integral results and measurements. However, the runback water flow distributions were close to each other since the mean temperature level predicted by both models are very close despite local temperature deviations. The present paper's differential model estimated initial freezing rates as 0.29 e 0.33 g/s in lower and upper surface. Similarly, the integral model predicted 0.26 e 0.31 g/s.

The mass conservation of runback water flow is presented in Tables 5, 6 and 7, for cases 22A, 67A and 67B. The difference ($\dot{m}_{evap} - \dot{m}_{imp}$) indicates the anti-ice system operating regime: 1) zero or less than $|1E-15|$, if it is evaporative; 2) equal to $\dot{m}_{water}$, if the runback flows downstream past the protected area but does not freeze; and 3) equal to $\dot{m}_{ice}$, if the runback flows downstream the protected area and freezes. The final position of impingiment s_{imp} and the final position of runback flow, s_{dry}, by evaporation or frezing are also presented in the same tables.

XI. Conclusions

In sum, the present paper fulfilled modeling blanks left by previous works of present and other authors by implementing models for surface wetness, boundary layer differential analysis and laminar-turbulent transition prediction in an airfoil thermal anti-ice numerical simulator. The differential analysis results considered the effects of flow history related to the surface temperature gradient, variation of the flow pressure gradient and the occurrence of laminar-turbulent transition. With the differential boundary-layer and rivulets

Table 5. Runback Mass Conservation - Case 22A

Diferential			Integral		
	upper	lower		upper	lower
$\dot{m}_{evap}$, kg/s	$0,266E-03$	$0,267E-03$	$\dot{m}_{evap}$, kg/s	$0,254E-03$	$0,255E-03$
$\dot{m}_{imp}$, kg/s	$0,266E-03$	$0,267E-03$	$\dot{m}_{imp}$, kg/s	$0,254E-03$	$0,255E-03$
$(\dot{m}_{evap}-\dot{m}_{imp})$, kg/s	$-0,542E-19$	$0,108E-18$	$(\dot{m}_{evap}-\dot{m}_{imp})$, kg/s	$0,000E+00$	$-0,542E-19$
$\dot{m}_r$, kg/s	$0,000E+00$	$0,000E+00$	$\dot{m}_r$, kg/s	$0,000E+00$	$0,000E+00$
$\dot{m}_{ice}$, kg/s	$0,000E+00$	$0,000E+00$	$\dot{m}_{ice}$, kg/s	$0,000E+00$	$0,000E+00$
s_{imp}/c	$0,267E-01$	$-0,285E-01$	s_{imp}/c	$0,270E-01$	$-0,290E-01$
s_{dry}/c	$0,243E-01$	$-0,231E-01$	s_{dry}/c	$0,250E-01$	$-0,250E-01$

Table 6. Runback Mass Conservation - Case 67A

Diferential			Integral		
	upper	lower		upper	lower
$\dot{m}_{evap}$, kg/s	$0,533E-03$	$0,533E-03$	$\dot{m}_{evap}$, kg/s	$0,522E-03$	$0,522E-03$
$\dot{m}_{imp}$, kg/s	$0,533E-03$	$0,533E-03$	$\dot{m}_{imp}$, kg/s	$0,522E-03$	$0,522E-03$
$(\dot{m}_{evap}-\dot{m}_{imp})$, kg/s	$-0,108E-18$	$0,108E-18$	$(\dot{m}_{evap}-\dot{m}_{imp})$, kg/s	$-0,108E-18$	$0,000E+00$
$\dot{m}_r$, kg/s	$0,000E+00$	$0,000E+00$	$\dot{m}_r$, kg/s	$0,000E+00$	$0,000E+00$
$\dot{m}_{ice}$, kg/s	$0,000E+00$	$0,000E+00$	$\dot{m}_{ice}$, kg/s	$0,000E+00$	$0,000E+00$
s_{imp}/c	$0,368E-01$	$-0,368E-01$	s_{imp}/c	$0,369E-01$	$-0,369E-01$
s_{dry}/c	$0,685E-01$	$-0,661E-01$	s_{dry}/c	$0,767E-01$	$-0,741E-01$

model, which was presented herein, the surface temperatures were closer to experimental data than integral boundary-layer and rivulets model, which was implemented in previous paper, predictions for cases 22A and 67B. For case 67A, both analyses predicted temperatures and heat transfer coefficients with equivalent accuracy. In order to approximate numerical code predictions to temperature measurement data, the anti-ice code with boundary-layer differential analysis required lower values of free stream turbulence levels than the one with integral analysis. The model presented herein was able to predict the laminar-turbulent transition process given an adjusted frestream turbulence level. The empirical correlations predicted the transition onset and end position around the airfoil, and the present model did not require to arbitrarly fixing of the transition region parameters. Therefore, the given an "equivalent" turbulence level, the model will predict the surface temperature and runback water distributions on upper and lower airfoil heated surfaces operating under icing conditions, zero angle of attack and conditions near those simulated herein.

XII. Acknowledgment

One of authors (G. A. L. da Silva) wishes to acknowledge Fundação de Amparo à Pesquisa do Estado de São Paulo (FAPESP) for the financial support received by the full time doctoral grant 07/00419-0 from July 2007 to February 2009. Also he acknowledges Prof. Dr. Marcos de Mattos Pimenta and Dr. Tuncer Cebeci for the recomendation that allowed G. A. L. Silva being visiting scholar at CSULB.

Table 7. Runback Mass Conservation - Case 67B

Diferential			Integral		
	upper	lower		upper	lower
$\dot{m}_{evap}$, kg/s	$0,508E-03$	$0,508E-03$	$\dot{m}_{evap}$, kg/s	$0,508E-03$	$0,508E-03$
$\dot{m}_{imp}$, kg/s	$0,218E-03$	$0,175E-03$	$\dot{m}_{imp}$, kg/s	$0,243E-03$	$0,199E-03$
$(\dot{m}_{evap}-\dot{m}_{imp})$, kg/s	$0,290E-03$	$0,334E-03$	$(\dot{m}_{evap}-\dot{m}_{imp})$, kg/s	$0,265E-03$	$0,309E-03$
$\dot{m}_r$, kg/s	$0,000E+00$	$0,000E+00$	$\dot{m}_r$, kg/s	$0,000E+00$	$0,000E+00$
$\dot{m}_{gelo}$, kg/s	$0,290E-03$	$0,334E-03$	$\dot{m}_{gelo}$, kg/s	$0,265E-03$	$0,309E-03$
s_{ice}/c	$0,115E+00$	$-0,104E+00$	s_{ice}/c	$0,113E+00$	$-0,101E+00$
s_{imp}/c	$0,384E-01$	$-0,384E-01$	s_{imp}/c	$0,384E-01$	$-0,384E-01$
s_{dry}/c	$0,115E+00$	$-0,104E+00$	s_{dry}/c	$0,113E+00$	$-0,101E+00$

References

[1]Silva, G. A. L., *Modelagem e simulação da operação de sistema antigelo eletrotérmico de um aerofólio*, Master's thesis, Escola Politécnica da Universidade de São Paulo, São Paulo, SP, Brazil, April 2002.

[2]Botura, G., Flosdorf, D., and Sweet, D., "Concept Development of Low Power Electrothermal De-icing System," *AIAA Paper 2006-864*, AIAA Aerospace Sciences Meeting and Exhibit, 46th, 2008, Reno, American Institute of Aeronautics and Astronautics, Reston, January 2008.

[3]Elangovan, R. and Olsen, R., "Analysis of Layered Composite Skin Electro-Thermal Anti-Icing System," *AIAA Paper 2008-446*, AIAA Aerospace Sciences Meeting and Exhibit, 46th, 2008, Reno, American Institute of Aeronautics and Astronautics, Reston, January 2008.

[4]Silva, G. A. L., *Transferência de Calor e de Massa no Escoamento Bifásico em torno de aerofolios equipados com sistemas de antigelo aeronáuticos*, Ph.D. thesis, Escola Politécnica da Universidade de São Paulo, São Paulo, SP, Brazil, Fevereiro 2009.

[5]Al-Khalil, K. M., *Numerical simulation of a an aircraft anti-icing system incorporating a rivulet model for the runback water*, Ph.D. thesis, University of Toledo, Toledo, Ohio, USA, 1991.

[6]Wright, W. B., *User Manual for the Improved NASA Lewis Ice Accretion Code LEWICE 1.6*, National Aeronautics and Space Administration, Cleveland, May 1995, 95 p. (Contractor Report, 198355).

[7]Guffond, D. and Brunet, L., *Validation du programme bidimensionnel de capitation*, Office National D'Études et de Recherches Aérospatiales, Châtillon Cedex, France, 1988, (Rapport Technique , RP 20/5146 SY).

[8]Gent, R., *TRAJICE2 - A Combined Water Droplet Trajectory and Ice Accretion Prediction Program For Aerofoils*, Royal Aerospace Establishment, Farnborough, 1990, (Technical Report, 90054).

[9]Silva, G. A. L., Silvares, O. M., and Zerbini, E. J. G. J., "Aircraft Wing Electrothermal Anti-icing: Heat and Mass Transfer Effects," *Proceedings of Eurotherm*, 5th European Thermal-Sciences Conference, Eindhoven, Begell House, Inc., New York, May 2008.

[10]Cebeci, T., "Essential ingredients of a method for low reynolds-number airfoils," *AIAA Journal*, Vol. 27, No. 12, 1989, pp. 1680–1688.

[11]Cebeci, T., Chen, H. H., and Alemdaroglu, N., "Fortified LEWICE with Viscous Effects," *Journal of Aircraft*, Vol. 28, No. 9, Setembro 1991, pp. 564–71.

[12]Morency, F., Tezok, F., and Paraschivoiu, I., "Anti-icing System Simulation Using CANICE," *Journal of Aircraft*, Vol. 36, No. 6, 1999.

[13]Henry, R., *Development of an electrothermal de-icing/anti-icing model*, Office National d'Etudes et de Recherches Aérospatiales, Chatillon Cedex, 1992, (Rapport ONERA TAP, 92005).

[14]Cebeci, T., Chen, H., Kaups, K., Schimke, S., and Shin, J., *Analysis of Iced Wings*, National Aeronautics and Space Administration, Washington, January 1992, 16 p. (Technical Memorandum, 105773).

[15]Cebeci, T. and Bradshaw, P., *Physical and Computational Aspects of Convective Heat Transfer*, Springer-Verlag, New York, 1984.

[16]Chen, K. K. and Thyson, N. A., "Extension of Emmon's spot theory to flows on blunt bodies," *AIAA Journal*, Vol. 9, No. 5, 1971.

[17]Al-Khalil, K. M., Horvath, C., Miller, D. R., and Wright, W., *Validation of NASA thermal ice protection computer codes. Part 3 - Validation of ANTICE*, National Aeronautics and Space Agency, Cleveland, OH, May 2001, 18 p. (Contractor Report, 2001-210907).

[18]Michel, R., *Etude de la transition sur les profiles d'aile. Establissement d'un critére de Determination de Point de Transition et Calcul de la Trainee de Profile Incompressible*, Office National D'Études et de Recherches Aérospatiales, Chatillon Cedex, 1951, (ONERA Rapport, 1/1578A).

[19]Silva, G. A. L., Silvares, O. M., and Zerbini, E. J. G. J., "Airfoil anti-ice system modeling and simulation," *AIAA Paper 2003-734*, Aerospace Sciences Meeting and Exhibit, 43., 2005, Reno, America Institute of Aeronautics and Astronautics, Reston, 2003.

[20]Silva, G. A. L., Silvares, O. M., and Zerbini, E. J. G. J., "Numerical Simulation of Airfoil Thermal Anti-ice Operation. Part 1: Mathematical Modeling," *Journal of Aircraft*, Vol. 44, No. 2, Março-Abril 2007, pp. 627–33.

[21]Silva, G. A. L., Silvares, O. M., and Zerbini, E. J. G. J., "Numerical Simulation of Airfoil Thermal Anti-ice Operation. Part 2: Implementation and Results," *Journal of Aircraft*, Vol. 44, No. 2, Março-Abril 2007, pp. 634–41.

[22]Ambrok, G. S., "Approximate Solution of Equations for the Thermal Boundary Layer with Variations in Boundary Layer Structure," *Soviet Physics - Technical Physics*, , No. 2, 1957, pp. 1979–86.

[23]Reynolds, W. C., Kays, W. M., and Kline, S. J., *Heat transfer in the turbulent incompressible boundary layer. IV - Effect of location of transtion and prediction of heat transfer in a known transition region*, National Aernautics and Space Administration, Washington, D.C., December 1958, (Memorandum, 12-4-58W).

[24]Cebeci, T. and Cousteix, J., *Modeling and computation of boundary-layer flows : laminar, turbulent and transitional boundary layers in incompressible and compressible flows*, Horizons Publishing, Long Beach, 2005.

[25]Mikielewicz, J. and Moszynski, J. R., "Breakdown of a shear driven liquid film," *Polzka Akademia Nauk. - Prace Instytutu Maszyn Przeplywowych*, , No. 66, 1975, pp. 3–11.

[26]Abu-Ghannam, B. and Shaw, R., "Natural Transition of Boundary Layers - The Effects of Turbulence, Pressure Gradient and Flow History," *Journal of Mechanical Engineering Science*, Vol. 22, No. 5, 1980, pp. 213–228.

[27]Silva, G. A. L., Silvares, O. M., and Zerbini, E. J. G. J., "Water Film Breakdown and Rivulets Formation Effects on Thermal Anti-ice Operation Simulation," *AIAA Paper 2006-3785*, AIAA/ASME Joint Thermophysics and Heat Transfer Conference, 9., 2006, San Francisco, America Institute of Aeronautics and Astronautics, Reston, June 2006.

[28]Silva, G. A. L., Silvares, O. M., and Zerbini, E. J. G. J., "Boundary-Layers Integral Analysis - Heated Airfoils in Ice Conditions," *AIAA Paper 2008-0475*, AIAA Aerospace Sciences Meeting and Exhibit, 46th, 2008, Reno, American Institute of Aeronautics and Astronautics, Reston, January 2008.

[29]Eckert, E. R. G., "Engineering Relations for Friction and Heat Transfer to Surfaces in High Velocity Flow," *Journal of the Aeronautical Sciences*, Vol. 22, 1955, pp. 585–587.

[30]Spalding, D. B., *Convective mass transfer, an introduction*, McGraw-Hill, New York, 1963.

[31]Kays, W. M. and Crawford, M. E., *Convective heat and mass transfer*, McGraw-Hill, New York, 1993.

[32]Pimenta, M. M., *The turbulent boundary layer: an experimental study of the transport of momentum and heat with the effects of roughness*, Ph.D. thesis, Stanford University, Stanford, May 1975.

[33]Mikielewicz, J. and Moszynski, J. R., "Minimum thickness of a liquid film flowing vertically down a solid surface," *Int. J. Heat and Mass Transfer*, Vol. 19, 1976, pp. 771–776.

[34]Silva, G. A. L., Silvares, O. M., and Zerbini, E. J. G. J., "Simulation of an Airfoil Electro-Thermal Anti-Ice System Operating in Running Wet Regime," *AIAA Paper 2005-1374*, Aerospace Sciences Meeting and Exhibit, 41., 2003, Reno, American Institute of Aeronautics and Astronautics, Reston, Janeiro 2005.

[35]Cebeci, T. and Smith, A., *Analysis of turbulent boundary layers*, Academic Press, 1st ed., 1974.

[36]Sogin, H. H., *A design manual for thermal anti-icing systems*, Wright Air Development Center Technical, Illinois, 1954, (Technical Report, 54-13).

[37]Gent, R. W., Dart, N. P., and Cansdale, J., "Aircraft Icing," *Phil. Trans. Royal Society London A*, , No. 358, 2000, pp. 2873–2911.

[38]Gent, R., Moser, R., Cansdale, J., and Dart, N., "The Role of Analysis in the Development of Rotor Ice Protection System," *SAE Paper 2003-01-2090*, FAA In-flight Icing, Ground De-icing International Conference & Exhibition, 1., Chicago, 2003, IL, Society of Automotive Engineers, Warrendale, June 2003.

[39]Kerho, M. F. and Bragg, M. B., "Airfoil Boundary-Layer Development and Transition with Large Leading-Edge Roughness," *AIAA Journal*, Vol. 35, No. 1, January 1997, pp. 75–84.

[40]Stefanini, L. M., Silvares, O. M., Silva, G. A. L., and Zerbini, E. J. G. J., "Boundary-Layers Integral Analysis - Airfoil Icing," *AIAA Paper 2008-0474*, AIAA Aerospace Sciences Meeting and Exhibit, 46th, 2008, Reno, America Institute of Aeronautics and Astronautics, Reston, January 2007.

[41]Tobaldini, Neto, L., Pimenta, M. M., and Silva, G. A. L., "Laminar-turbulent transition modeling strategies for thermally protected airfoils," *Proceedings of FEDSM2008*, 2008 ASME Fluids Engineering Conference, American Society of Mechanical Engineers, Reston, August 2008, pp. 1–9.

[42]Silva, G. A. L., Silvares, O. M., and Zerbini, E. J. G. J., "Integral Analyses of the Convective Heat Transfer around Ice Protected Airfoils," *Proceedings of CHT-08*, ICHMT International Symposium on Advances in Computational Heat Transfer, Marrakesh, International Centre of Heat and Mass Transfer, Ankara, May 2008.

[43]Henze, C. M., Bragg, M. B., and Kim, H. S., "Freestream Turbulence Measurements in Icing Condition," *AIAA Paper 1998-96*, Aerospace Sciences Meeting and Exhibit, 36., 1998, Reno, America Institute of Aeronautics and Astronautics, Reston, January 1998.